

# Imaging at Subsecond Rates with the ATA

Casey J. Law, David MacMahon, and Melvyn Wright

August 2009

## 1. Abstract

The flexible digital design of modern radio interferometers is enabling a wide range of new science. These new capabilities allow us to perform efficient surveys for transients faster than a second through “fast imaging”. This memo describes initial steps in commissioning fast imaging on the ATA. Observations of Cygnus A demonstrate the system performance on subsecond time scales. Observations of pulsar B0329+54 show that Jy-brightness transient radio sources can be detected with only a fraction of the full ATA-42 sensitivity.

## 2. Introduction

The study of transient radio sources is expanding rapidly with the development of new radio interferometers like the ATA. Most current work is focused on studying changes on time scales longer than minutes (Bower et al. 2004). The intent of this memo is to develop the techniques for studying radio transients faster than a second, hereafter called “fast transients”.

Fast transients, by their nature, are more likely to be caused by coherent, energetic processes. The physics probed at these time scales is diverse, since known fast radio transients include neutron star transients (pulsars, RRATs; McLaughlin et al. 2006), flare stars (Osten & Bastian 2008), and planets (Zarka et al. 2008).

Techniques for studying the time-domain on this time scale have been largely been done with dedicated instruments using single-dish radio telescopes. In cases where radio interferometers are used, they observe in “tied-array” mode, forming a single beam on the sky. However, the capacity to image with radio interferometers can effectively form hundreds of tied-array beams. This new mode of observing could open more efficient methods of surveying for transients.

The techniques for fast imaging have not been fully developed. Most correlators output data with sample rates slower than 10s, which dramatically reduces sensitivity to fast transients. The principal reason for this is to reduce the volume of data, which is already

significant for survey instruments like the ATA. Slow integrations also allow one to ignore effects of the ISM (e.g., dispersion). However, newer correlators are being designed with high sample rates to improve the flagging of RFI. This capability can be used for new science.

This memo describes the commissioning of a fast imaging mode on the ATA. The necessary software changes in the data catcher are described in §3. An initial test the fast imaging mode on Cygnus A, and ATA system stability is described in §4. In §5, we show the results of fast imaging of a bright pulsar, B0329+54. Conclusions and future directions are given in §6.

### 3. Catching Fast Imaging Data

While correlators sample visibilities at rates comparable to the frequency of the electromagnetic wave, they integrate over longer time scales to reduce the data volumes. In the case of the ATA, the 64-input FX correlator has a fundamental integration unit of 10 ms and a default integration time is 10 s (Urry et al. 2007). For the “fxmir” data catcher, an integration with all 42 antennas and 512 channels takes about 5 s to write. An integration time of 10 s is used to allow some variation in the dump time.

To push the integration times into the “fast imaging” time scales, the fxmir catcher was modified to allow dumping fewer than the full 512 channels (per spectral half). Combining this capability with observations of fewer than the full 42 antennas, allows further flexibility in the amount of data dumped to disk.

To calibrate the rate at which the data catcher can safely write correlator data, we observed with a range of system configurations. We varied the number of antennas from 21 to 42 antennas and the number of channels from 1 to 512. We found linear trends in the dump times as a function of the numbers of baselines and channels. A good fit to the dump times is:

$$t_{\text{dump}} = (0.6\text{s} + 4.0\text{s} * f_{\text{ch}}) * f_{\text{bl}} \tag{1}$$

where  $f_{\text{ch}}$  is the fractional number of channels (relative to 512), and  $f_{\text{bl}}$  is the fractional number of baselines (relative to the full 42-element array). The dump time approaches a lower limit at small numbers of channels because the header is a lower limit to the data volume per integration.

We used this relation to define the optimal system configuration of 32 channels and 8

antennas to reliably reach integration times of 100 ms. In practice, this number can vary between individual integrations, since the data dump time depends on the HCRO LAN network speed.

#### 4. Fast Imaging of Cygnus A

It was not clear that the array performance at subsecond speeds would be the same as during normal operation. In particular, we were interested in the calibration stability and noise properties on these short time scales. We observed Cygnus A, a bright calibrator, to study the system performance.

In February 2009, we observed Cygnus A with one correlator at 1.4 GHz. We used the `fxmir` data catcher to integrate data with 32 channels from seven antennas at a rate of 0.2 s. We selected antennas from a compact configuration to assure that Cygnus A is unresolved. A total of 10 min of data was recorded and none of the integrations took longer than the dump time to write.

We self-calibrated each integration assuming Cygnus A was a point source with flux density of 1400 Jy. This process should move all antenna-based gains into the gain solution and leave baseline-based problems in the data. To first order, the gains are mostly antenna based. A crude way to demonstrate this is by imaging each calibrated integration, as shown in the movie at <http://log.hcro.org/content/movie-cyg-a-with-02s-resolution>.

A better test of calibration quality is to view the data after applying the solution. Figure 1 shows the calibrated data amplitude. Note that since we applied self-calibration to each integration, each baseline should have an amplitude of exactly 1400 Jy; variations from 1400 Jy indicate a problem with the self-calibration model (i.e., a baseline-based error). In general, each baseline has a flux density that is unchanging in time and within 10% of 1400 Jy.

The calibration solutions show phase and amplitude structure on time scales shorter than 10 s. Figure 2 shows the gain amplitude solution for the seven antennas. The gain amplitude generally changes slowly over the 10 min observation. Two antennas (13 and 15) show 10% variations in the gain amplitude on 10 s time scales. The changes in these antennas are at the same time (within a few seconds), but have very different structure. A 10% gain amplitude error is equivalent to a pointing error of 0.6 times the half power radius ( $\approx 75$  at 1.4 GHz), assuming a Gaussian primary beam. The origin of these changes are not clear, but if sampled at slower integration times, they could be interpreted as noise or interference.

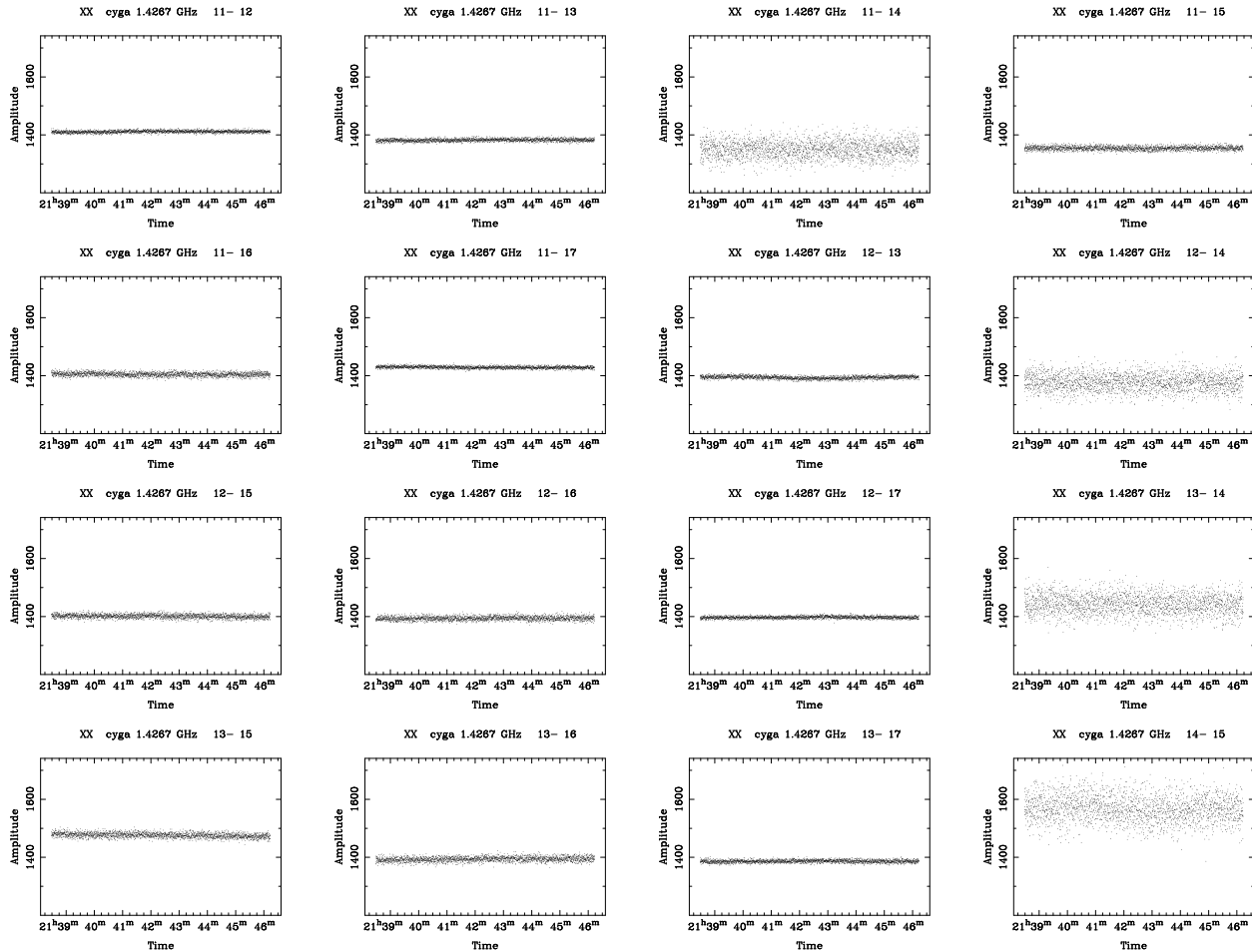


Fig. 1.— The data amplitude for a selection of baselines from the fast imaging observation of Cygnus A. The data were self-calibrated on each integration assuming a flux density of 1400 Jy for Cygnus A. Cygnus A is unresolved by all baselines used in this observation.

The gain phase solution shown in Figure 3 has a more complex structure than the gain amplitude. Phases generally vary by only a few degrees; Antenna 13 has a dip of about  $3^\circ$  at the same time as its gain amplitude event. More interesting is the coherent variation in the gain phase as a function of time. Each antenna phase has a ragged variation with amplitude of about  $2^\circ$  on a time scale 30 s to 1 min.

The origin of this phase wobble is not clear. If it is antenna based, then it could indicate the effect of motion of the antenna drive system or errors in fringe rotation. However, this day was not particularly windy (10 mph) and the drives do not have a 30 s time scales. Fringe rotation errors would tend to arise at time scales of 10 s, the period for updating the ibobs. Since the observation was during the day, the most likely explanation for the wobble

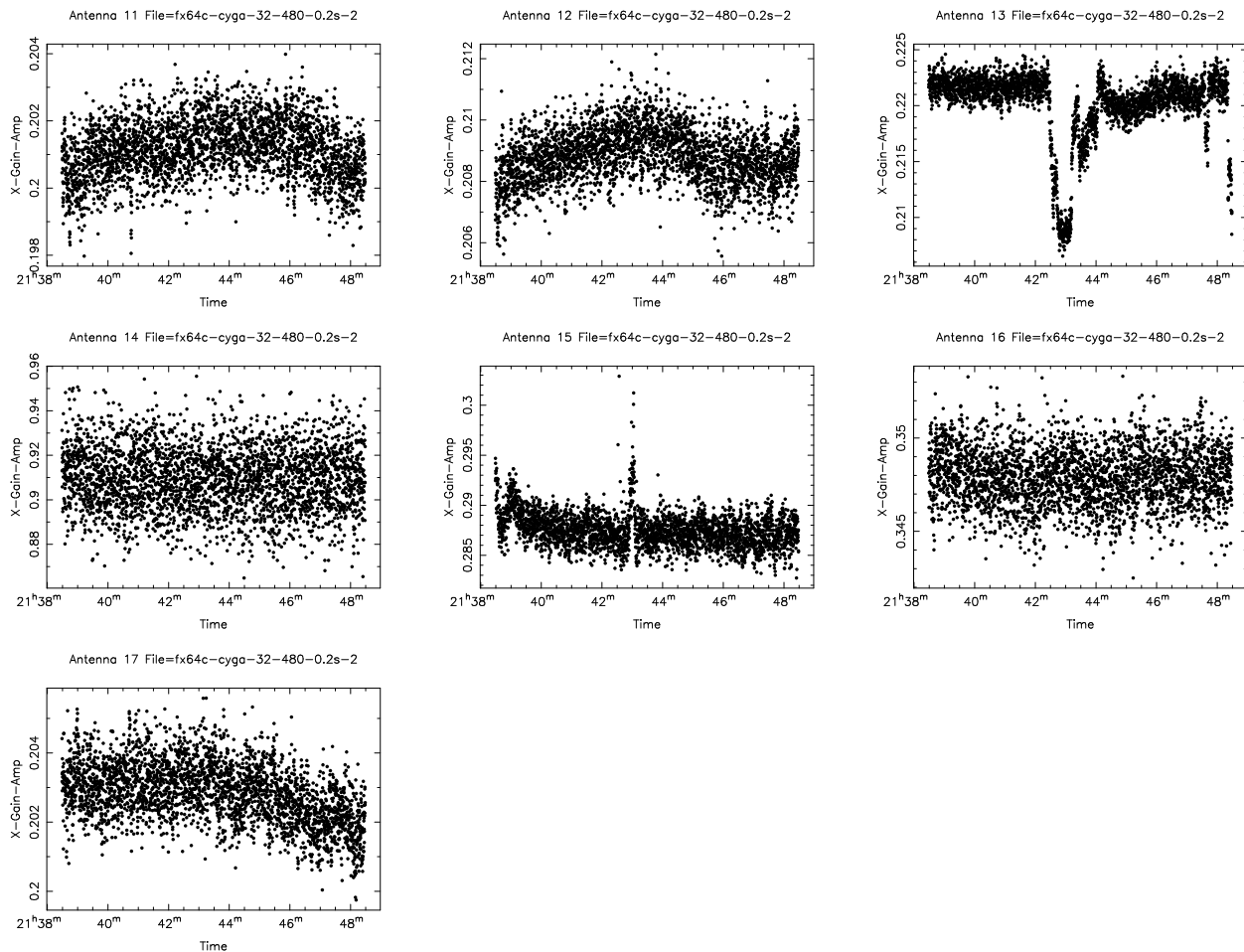


Fig. 2.— Plot of the gain amplitude for the x-pol of each antenna in the fast imaging observation of Cygnus A. The gain solution comes by self-calibrating each 0.2 second integration. Only seven antennas were included in the observation.

is that the sun was in a sidelobe. While this is a baseline-based error, it could appear in the gain solution if it is shared by many antennas. The antenna with the largest phase wobble (antenna 17) also happens to have many baselines of similar distance (100 m); the fringe rate for this baseline for a source at the horizon is about 1/min, similar to the phase wobble. Regardless of its origin, this phase wobble will not be resolved for slower integration times. As such, it would be interpreted as noise and decorrelation in the data.

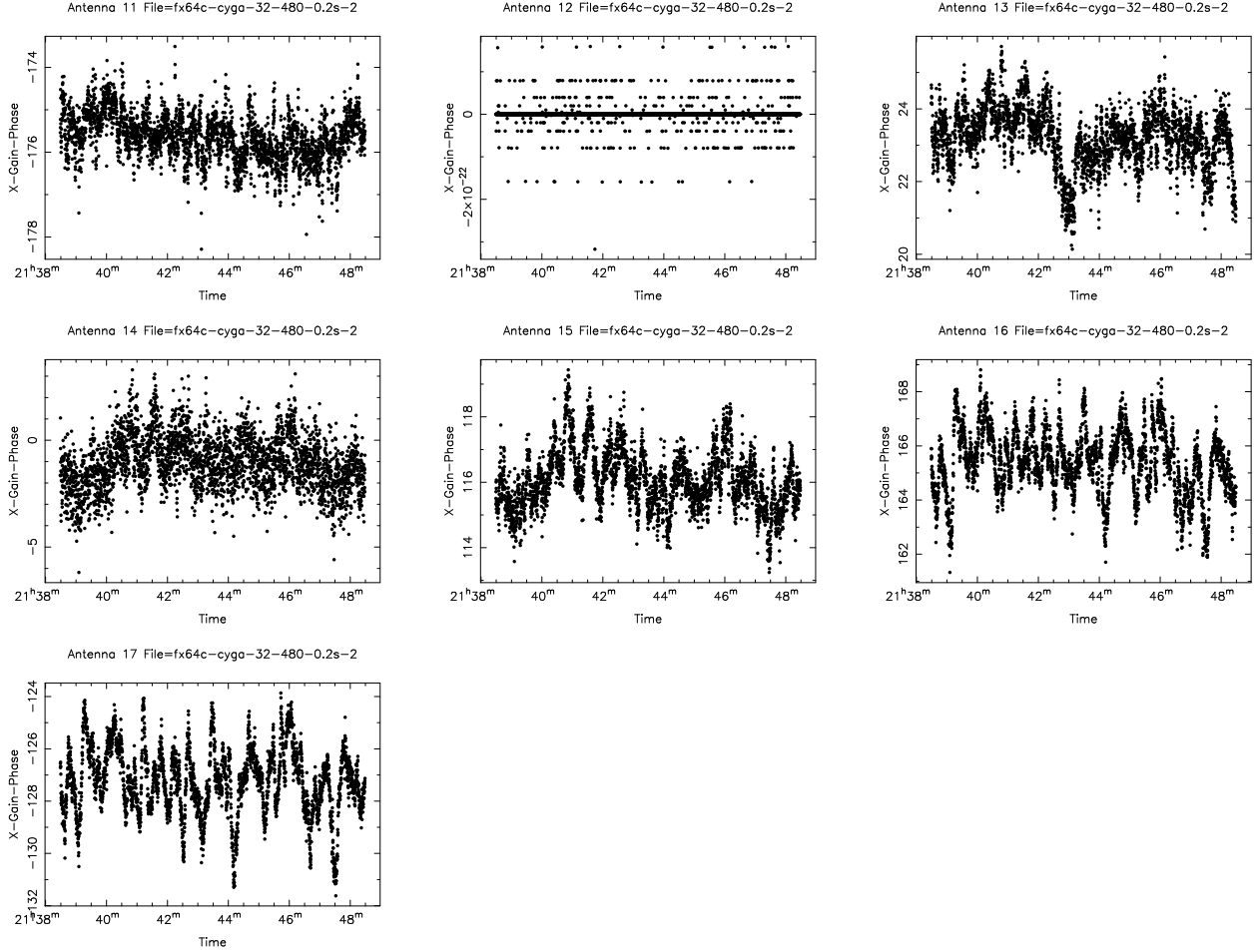


Fig. 3.— Plot of the gain phase for the x-pol of each antenna in the fast imaging observation of Cygnus A, as in Fig. 2.

### 5. Fast Imaging of B0329+54

One of the goals of the fast imaging observing mode is to find transients. A useful test in demonstrating this possibility is observing a known pulsar, which motivates writing analysis scripts and would test the absolute timing of the correlator data.

To demonstrate the fast imaging mode, we observed the pulsar B0329+54 on March 10, 2009. B0329+54 is the brightest pulsar visible to the ATA, with a mean flux density higher than 0.5 Jy below 1 GHz. Its period of 0.7 seconds is accessible to the ATA, if dumping a subset of the data. Our sensitivity estimates suggested that we would need to average about 30 pulses to detect B0329+54 in a 0.1 s bin at 700 MHz.

We observed with 32 channels and five antennas to reduce the dump time below 100 ms.

We found that the dump time was often shorter than 30 ms, but on four occasions the system slowed enough to that the data was not dumped faster than the integration time; the effect of integrating before dumping the previous integration is discussed below. The total integration time was 5 minutes. For gain calibration, we made a similar observation of Cassiopeia A.

The result of the observation is a standard visibility data set. We flagged data by eye (not much required) and did gain calibration based on the average solution toward Cassiopeia A. To image the average pulsed emission required custom scripts using Miriad (available in the MMM code repository under “claw/psr-\*”). The script assumes a pulse period to define pulse phase bins throughout the observation. This filter selects based on time stamps on the integrations, which are only given to 0.1 s precision. We then image each bin, which shows the average emission in that pulse phase bin. The dirty image is cleaned lightly and restored. In the case of B0329+54, eight bins were defined across the pulse phase (slightly overresolving the pulse). The mean of the eight pulse bin images was subtracted from the individual pulse bin images to remove confusion by other sources.

The images of the eight bins across the average pulse phase assuming a period of 0.71367 s are shown in Figure 4 and as a movie on the ATA logbook at <http://log.hcro.org/content/movie-b032954-100ms-resolution>. At phase bin 5, a point source with flux density of about 5.7 +- 0.2 Jy is seen at the position of B0329+54. The flux density of the source is consistent with the predicted value at this time resolution and frequency. No constant sources of this flux density are known at this location. Note that subtracting the average emission makes a weak negative artifact at off-peak pulse phases.

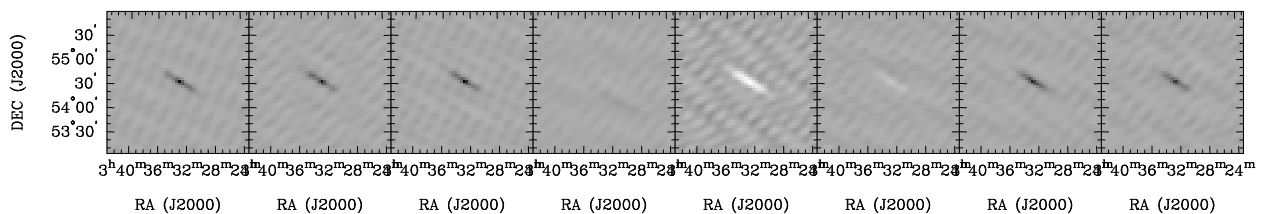


Fig. 4.— Images of eight bins across the pulse profile of B0329+54. Each image shows the average emission during a 5 minute observation, assuming a period of 0.71367 s. The pulsed emission happens to fall in pulse bin 5, while most other bins show a negative artifact of the subtraction of the mean pulse profile.

A reader familiar with B0329+54 will recognize that the period that produces the nice result reported above is not the period of B0329+54. Imaging at the reported period of 0.714520 s produces a 1.5 Jy detection of the pulsar, much less than expected. Furthermore, imaging the data in pieces at the known period shows a drift of the pulse phase with time,

suggesting that the period is wrong. The Doppler effect for this time and direction predicts a drift of  $1.6 \times 10^{-4} \text{ s s}^{-1}$ , which is about 8 times smaller than observed. A more likely explanation is that the period drift is related to the four integrations that may have been overwritten before the data was dumped. The pulse drift rate is equal to the overwritten integration time relative to the observation length ( $0.4 \text{ s}/300 \text{ s} = 1.2 \times 10^{-3}$ ). Observations with a different number of overwritten integrations are needed to show this conclusively.

The analysis scripts allow rapid imaging of the pulse profile for a range of assumed periods. This let us fit for the best period of the pulsar based on either the drifting of pulse bin or maximal signal to noise ratio. In the case of B0329+54, we fit the pulsar period to a precision of  $2.2 \times 10^{-4} \text{ s}$ .

As it turns out, B0329+54 is not only bright, but has large variations in pulse-to-pulse brightness. This makes it a good target to image individual pulses. By dividing the data in time and repeating the pulse profile image script, we found that we could detect pulses in individual integrations. A second set of analysis scripts were written to study the change of pulses in a pulse phase bin with time (in the MMM code repository under “claw/psrbin-\*”).

Knowing the timing of the pulsar from the previous work, we imaged the phases when the pulsar was known to be on (the “on pulse”). A series of images of the on pulse for B0329+54 is shown in Figure 5 and in a movie at <http://log.hcro.org/content/movie-individual-pulses-b032954>. Each frame is different, with the brightest pulse detected at 40 Jy (seen in frame 20), while the faintest are below the detection limit of roughly 2 Jy. This variation is consistent with previous observations that predict a typical peak flux density of about 5 Jy at 700 MHz, but with wide variation between pulses (Kramer et al. 2003).

## 6. Conclusions

This memo demonstrates the use of the ATA correlator with integrations faster than 1 s. The goal of this campaign is to demonstrate the possibility of studying subsecond transients and source variability.

A relatively small amount of work is needed to enable integration times shorter than a second. With the current design, integration times of about 0.1 s are possible if a subset of 32 channels and 7 antennas are used. Reducing the amount of data or header information dumped could speed the data catcher. Since these tests were done, optimizations were proposed for the fxmir catcher that could speed the data rates by up to a factor of 2.

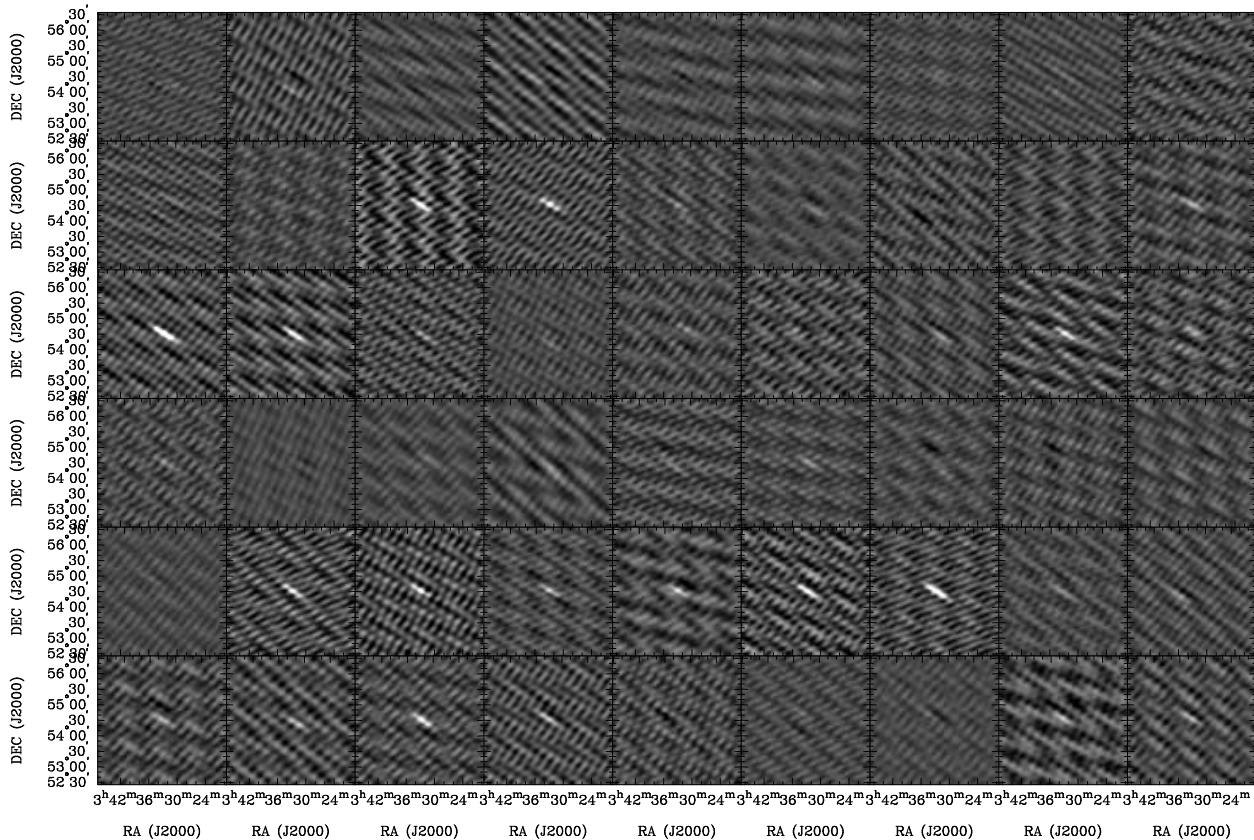


Fig. 5.— Images of the first 54 on pulses of B0329+54 at 700 MHz. The on pulse is found by assuming a pulsar period and phase from the fit across the entire five minute observation. The brightest pulse has a flux density of about 40 Jy and is shown in the 20th panel. The typical noise level in the images is about 1 Jy. The noise is not necessarily thermal, since it likely has a contribution from imperfect subtraction of the brighter, off pulse emission.

Observations of the bright, calibrator Cygnus A show that much of the system changes on second timescales can be calibrated into the antenna-based gains. After correcting for these gains, residuals of less than 10% are observed in the data. The gain phases show sawtooth-like wobbles of a few degrees on timescales of about a minute. The origin is not clear, but is consistent with the effect of a bright source in the sidelobe. On longer integration times, this phase wobble could be interpreted as an extra source of noise. With more baselines, these sidelobe effects will be reduced.

Observations of the bright pulsar B0329+54 show that the average pulse profile and individual pulses can be detected. Typical peak sensitivity is 0.2 Jy for the average profile in 300 s and integration time of 0.1 s. The sensitivity to individual pulses is roughly 1 Jy. A timing error was detected by fitting the best pulse period to B0329+54. The error is

consistent with the combination of the Doppler effect and overwritten integrations during a few slow data dumps.

Dual correlator observations could help answer open questions. Fast imaging with different antenna selection would determine if the phase wobble is caused by a sidelobe. Such an observation could also measure the scale of the error introduced by periodic updates of the fringe rotator. Timing of pulsars with two correlators could test the idea that the timing error is caused by dropped integrations.

The sensitivity of the array limits future work to only a handful of pulsars, though improvements to the data catchers may extend this slightly. Integration times below 100 ms are needed to start studying dispersion and scattering effects. We note that parts of myriad assume uv data time precision of 100 ms, so changes may be needed. These effects are useful diagnostics of transients and are necessary to enable the potential of fast imaging in large surveys.

## REFERENCES

- Bower, G. C., Falcke, H., Herrnstein, R. M., Zhao, J.-H., Goss, W. M., Backer, D. C. 2004, *Science*, 304, 704
- Kramer, M. et al. 2003, *A&A*, 407, 655
- Urry, W. L., Wright, M. C. H., Dexter, M. & MacMahon, D. 2007, *ATA memo series*, 73
- McLaughlin, M. A. et al. 2006, *Nature*, 439, 817
- Osten, R. A. & Bastian, T. S. 2008, *ApJ*, 674, 1078
- Zarka, P., Farrell, W., & Fischer, G., & Konovalenko, A. 2008, *SSRv*, 137, 257